



Structure of rotational bands in  $^{109}\text{Rh}$ A. J. Majarshin <sup>1</sup>, Yan-An Luo,<sup>1</sup> Feng Pan,<sup>2,3</sup> and H. T. Fortune <sup>4</sup><sup>1</sup>*School of Physics, Nankai University, Tianjin 300071, People's Republic of China*<sup>2</sup>*Department of Physics, Liaoning Normal University, Dalian 116029, People's Republic of China*<sup>3</sup>*Department of Physics and Astronomy, Louisiana State University, Baton Rouge, Louisiana 70803-4001, USA*<sup>4</sup>*Department of Physics and Astronomy, University of Pennsylvania, Philadelphia, Pennsylvania 19104, USA*

(Received 5 March 2021; accepted 29 June 2021; published 28 July 2021)

Rotational bands in  $^{109}\text{Rh}$  are investigated in a simple model and in the interacting boson-fermion model. We have developed a solvable extended transitional Hamiltonian by adding a two-configuration mixing term. Results suggest that  $^{109}\text{Rh}$  is a good candidate for triaxiality and shape coexistence. Mixing between  $3/2^+$  states with  $K = 1/2$  and  $3/2$  is found to be weak, as evidenced by the  $E2$  strengths.

DOI: [10.1103/PhysRevC.104.014321](https://doi.org/10.1103/PhysRevC.104.014321)

## I. INTRODUCTION

Arima and Iachello proposed the original version of the interacting boson model (IBM) for even-even nuclei [1–4]. The extension of this model to the interacting boson-fermion model (IBFM) has been quite successful in odd mass nuclei [5–11]. In the neutron-rich region ( $40 \leq Z \leq 50$  and  $N \geq 50$ ), odd- $A$  Rh nuclei such as  $^{109}\text{Rh}$  (with  $Z = 45$ ,  $N = 64$ ) are of current interest because of the different deformation types they exhibit. Different shapes (e.g., prolate, oblate, and gamma-soft or triaxial) can coexist in the same nucleus [12–14]. Shape coexistence likely appears in a majority of nuclei. Examples of this coexistence phenomenon involving vibrational and rotational bands are seen from  $(\pi g_{9/2}, \pi p_{1/2}, \pi p_{3/2}, \pi f_{5/2})$  and  $(\pi g_{7/2}/d_{5/2})$  subshells, respectively, in the region of the  $Z = 50$  shell closure [15–17]. The  $A \approx 100$  region is renowned for the presence of normal and intruder states with different types of deformation. In this region ( $Z \geq 44$ ), the intruder states may originate from the top of the  $\pi g_{9/2}$  subshell with oblate deformation. To the contrary, the intruder states may originate below or near the bottom of the  $\nu h_{11/2}$  subshell with prolate deformation. In the nuclear potential system, prolate deformation decreases to become  $\gamma$ -soft or triaxial when the number of protons increases, away from the midshell. Moreover, when more neutrons are added, with strong softness and deformation, oblate deformation increases, and ground states become triaxial as we reach  $N = 60$  and beyond [18,19]. In Rh isotopes, we have the same phenomenon. It has been shown that there is clear evidence for shape coexistence based on the rotational band structure (intruder states) [20]. The interpretation of shape coexistence and shape transitions [21] for Rh isotopes, indicating the softness in the  $\gamma$  direction, is supported by the  $O(6)$  limit of the IBM and triaxial shape for the ground state [22].

The presence of  $K = 1/2$  intruder states in our model is well known. Some band mixing is inevitable, particularly to understand the  $B(E2)$  values. Previous studies have used

extensive spectroscopic information to analyze these intruder states built on the single  $1/2^+$  [431],  $3/2^+$  [422], and other Nilsson orbitals, which are very close to the Fermi level for  $Z = 45$  nuclei [16,23,24]. Therefore, these kinds of states are good candidates to investigate rotational bands in odd-mass nuclei. Such a concept has been simply extended to the Rh ( $Z = 45$ ) isotopes. Similar studies for other odd-mass nuclei were reported in the  $A \approx 100$  region [25–27]. For the odd- $A$  Rh nuclei in this region, several rotational bands are built on the single-particle levels with the odd proton occupying the  $\pi g_{9/2}$ ,  $\pi p_{1/2}$ , and  $\pi (g_{7/2}/d_{5/2})$  subshells [22,27]. In addition to the references cited herein for the Ru-Rh region, several workers investigated collective features in somewhat lighter nuclei. These include Ge and Se [28], Zr [29,30], and Mo [31,32]. Wood, *et al.* [33] discussed shape coexistence in even-even nuclei from  $^{16}\text{O}$  to  $^{238}\text{U}$ . An excellent review [34] on various aspects of coexistence did not mention  $^{109}\text{Rh}$ .

Recently, prominent solvable models were suggested for the IBM in even-even nuclei [35–41]. The aim of the present study is to extend and complete those kinds of solutions, proposing a solvable model for identifying band mixing. We have employed a two-configuration mixing plus pairing model [42,43] to calculate the collective bands' energy spectra and band mixing. We have also considered the  $E2$  strengths in a simpler model [44–46]. Details of the pairing model can be found in Refs. [41,42,47,48]. The main reason to include the configuration mixing Hamiltonian is we may not interpret the coexistence and intruder pattern without a two-configuration mixing term in the proposed model. These are especially useful when we have collective bands. The availability of experimental data has enabled us to study the quantum phase transition and  $E2$  transition rates within the intruder band and band mixing for shape coexistence in odd mass nuclei with vibrational- and rotational-like bands.

In the following, we present the available data, together with a simple analysis of the  $E2$  strengths. This is followed by model calculations within the IBFM framework.

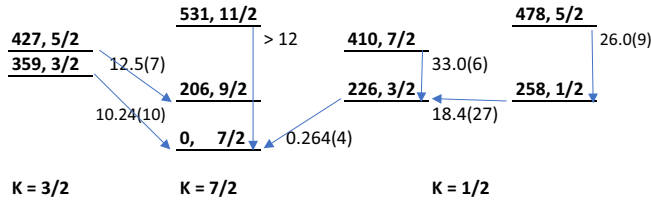


FIG. 1. Lowest members of first three rotational bands in  $^{109}\text{Rh}$ . The numbers by the arrows are  $M(E2)$ , computed from published E2 strengths [22] using the relationship  $M^2(i \rightarrow f) = (2J_i + 1)B(E2; i \rightarrow f)$ .

## II. DATA AND SIMPLE ANALYSIS

The low-lying positive-parity states of  $^{109}\text{Rh}$  divide themselves naturally into three bands: a  $K^\pi = 7/2^+$  ground band, a nearly degenerate, strongly decoupled  $1/2^+$  band, and a  $3/2^+$  side band. The latter is similar to the so-called gamma band in even-even nuclei. The  $7/2^+$  and  $1/2^+$  bands are supposedly built on the  $7/2^+$  [413] and  $1/2^+$  [431] proton Nilsson orbitals, respectively. The  $1/2^+$  band is frequently referred to as an intruder band. These band placements are illustrated in Fig. 1. The numbers by the arrows are  $M(E2)$ , computed from published E2 strengths [22] using the relationship  $M^2(i \rightarrow f) = (2J_i + 1)B(E2; i \rightarrow f)$ .

It can be noted that the E2 strength from the first  $3/2^+$  state to the  $7/2^+$  ground state (g.s.) is extremely small:  $B(E2) = 0.0174(5)$  W.u. Bucher *et al.* [22] suggested that this strong inhibition was caused by vastly different deformations for the two states. This is unlikely to be the case. The likely explanation is the fact that E2 transitions with  $\Delta K > 2$  are forbidden. The lower  $3/2^+$  state probably obtains its g.s. strength by mixing with the  $K^\pi = 3/2^+$  band head. We define basis states  $|JK\rangle = |3/2\ 1/2\rangle$  and  $|3/2\ 3/2\rangle$ . Then we write

$$\begin{aligned} |3/2(226\ \text{keV})\rangle &= a|3/2\ 1/2\rangle + b|3/2\ 3/2\rangle, \\ |3/2(359\ \text{keV})\rangle &= -b|3/2\ 1/2\rangle + a|3/2\ 3/2\rangle. \end{aligned} \quad (1)$$

Then  $b/a = M(226 \rightarrow \text{g.s.})/M(359 \rightarrow \text{g.s.}) = 0.264(4)/10.24(10) = 0.0258(1)$ , i.e., very little mixing. With this mixing, the potential matrix element causing the mixing is then about 3.43 keV. If the two  $5/2$  states mix with the same  $V$ , then their mixing amplitude is 0.0674, meaning the  $M$  from  $5/2(478)$  to  $9/2$  would be very weak.

In  $^{107}\text{Rh}$ , the E2 strength for the first  $3/2^+$  to  $7/2^+$  g.s. is much less inhibited:  $B(E2) = 0.16(2)$  W.u., compared to 0.0174 W.u. in  $^{109}\text{Rh}$ . This difference is easily understood from the different energy splittings of the lowest two  $3/2^+$  states in the two nuclei.

Within the  $K = 1/2^+$  band, the transition matrix elements scale as  $M(J_i 1/2 \rightarrow J_f 1/2) = M(1/2^+)(2J_i + 1)^{1/2}(J_i 1/2\ 20|J_f 1/2)$ , where the last factor is a Clebsch-Gordan coefficient, and  $M(1/2^+)$  is the same for all transitions within the band. Thus,  $M(7/2 \rightarrow 3/2)/M(5/2 \rightarrow 1/2)$  should be  $(12/7)^{1/2} = 1.31$ . The experimental ratio is 1.27(5). Similarly, the ratio  $M(1/2 \rightarrow 3/2)/M(1/2 \rightarrow 5/2)$  should be  $(2/3)^{1/2} = 0.816$ . The experimental ratio is 0.71(11). These results, and those for other transitions, are summarized in Table I.

TABLE I. E2 transition matrix elements [(W.u.) $^{1/2}$ ] within the  $K^\pi = 1/2^+$  band in  $^{109}\text{Rh}$ .

$i$	$f$	$M(E2)/M(1/2^+)$	$M_{\text{calc}}$	$M_{\text{exp}}^a$
5/2	1/2	1.095	26.0	26.0(9) <sup>b</sup>
3/2	1/2	0.8944	21.2	18.4(27)
5/2	3/2	0.5855	13.9	unknown
7/2	3/2	1.434	34.9	33.0(6)
7/2	5/2	0.4781	11.4	unknown

<sup>a</sup>Computed from published E2 strengths [22] using the relationship  $M^2(i \rightarrow f) = (2J_i + 1)B(E2; i \rightarrow f)$ .

<sup>b</sup>Normalizing this transition strength provides  $M(1/2^+) = 23.74(\text{W.u.})^{1/2}$ .

The lowest negative-parity states also appear to form a rotational band, having  $K^\pi = 1/2^-$ , presumably based on the proton Nilsson orbital  $1/2^-$  [301]. The known states in this band, and the known transition matrix element, are depicted in Fig. 2. A comparison of the  $5/2 \rightarrow 1/2$  matrix elements in the two  $K = 1/2$  bands indicates that the  $1/2^-$  band is somewhat less collective than the  $1/2^+$  band. Expected transition matrix elements for the  $1/2^-$  band are listed in Table II.

Transitions from the  $K = 3/2$  to  $7/2$  band have  $\Delta K = 2$ , and scale as  $M(J_i 3/2 \rightarrow J_f 7/2) = M(0(2J_i + 1)^{1/2}(J_i 3/2\ 22|J_f 7/2)$ . Thus, the ratio  $M(5/2\ 3/2 \rightarrow 9/2\ 7/2)/M(3/2\ 3/2 \rightarrow 7/2\ 7/2)$  should be 0.913. The experimental ratio is  $12.5(7)/10.24(10) = 1.22(7)$ . This enhancement of the  $5/2 \rightarrow 9/2$  transition could arise from the mixing of the  $9/2^+$  states in the  $3/2$  and  $7/2$  bands. The  $5/2 \rightarrow 9/2$  transition would gain strength from the  $9/2 \rightarrow 5/2$  in-band transition. The  $9/2$  member of the  $3/2$  band is currently unknown. A state at 1097 keV has a strong  $L = 4$  angular distribution in the  $^{110}\text{Pd}(d, ^3\text{He})$  reaction, with  $C^2S = 1.8$  [20]. By comparison, the first  $9/2^+$  state has  $C^2S = 3.4$ , whereas the  $7/2^+$  g.s. is understandably weak, with  $C^2S = 0.19$ . The  $9/2^+$  assignment is confirmed from the analyzing power in the  $^{110}\text{Pd}(t, \alpha)$  reaction with polarized tritons [49]. The only known decays of the 1097-keV state are to states with  $J^\pi = 7/2^+, 9/2^+$ , and  $11/2^+$ , presumably via M1. A measurement

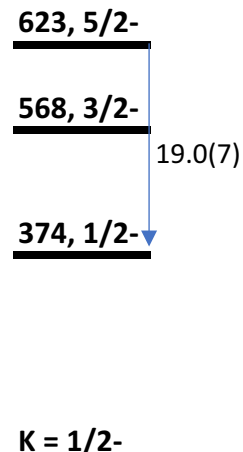


FIG. 2. As in Fig. 1, but for a negative-parity band.

TABLE II. E2 transition matrix elements  $[(W.u.)^{1/2}]$  within the  $K^\pi = 1/2^-$  band in  $^{109}\text{Rh}$ .

$i$	$F$	$M(E2)/M(1/2^-)$	$M_{\text{calc}}$	$M_{\text{exp}}$
5/2	1/2	1.095	19.0	19.0(7) <sup>a</sup>
3/2	1/2	0.8944	15.5	
5/2	3/2	0.5855	10.2	
7/2	3/2	1.434	24.9	
7/2	5/2	0.4781	8.30	

<sup>a</sup>Normalizing this transition strength provides  $M(1/2^-) = 17.35(W.u.)^{1/2}$ .

of the E2 strength from this state to the  $5/2^+$  member of the  $K = 3/2$  band would be valuable. Hagen *et al.* [50] report strong mixing between the  $11/2^+$  member of the g.s. band and a supposed ( $11/2^+$ ) band head at 642 keV.

### III. THEORETICAL FRAMEWORK

#### A. Theory of IBFM

The theory of building blocks for IBM is based on the  $s$  and  $d$  boson numbers with angular momentum of  $L = 0$  and 2 [1–4]. In a first attempt at describing the energy spectra built on the intruder state, we have chosen a transitional Hamiltonian by adding a two-configuration mixing term. It has been shown that  $U(5)$  and  $O(6)$  configurations are the basic ingredients to reproduce the normal and intruder states, respectively [51]. The group chain associated with the normal  $U(5)$  limit is

$$U(6) \supset U(5) \supset O(5) \supset O(3). \quad (2)$$

$[N] \quad \{n_d\} \quad \nu \quad L$

The relevant chain associated with the intruder  $O(6)$  limit is

$$U(6) \supset O(6) \supset O(5) \supset O(3). \quad (3)$$

$[N+2] \quad (\sigma) \quad \tau \quad L$

We introduce the generators of quasispin operators [35,37,41,52] with

$$\hat{S}_s^+ = (\hat{S}_s^-)^\dagger = \frac{1}{2}s^{\dagger 2}, \quad \hat{S}_s^0 = \frac{1}{4}(s^\dagger s + s^\dagger s), \quad (4)$$

$$\hat{S}_d^+ = (\hat{S}_d^-)^\dagger = \frac{1}{2}d^\dagger d^\dagger, \quad \hat{S}_d^0 = \frac{1}{4} \sum_\mu (d_\mu^\dagger d_\mu + d_\mu d_\mu^\dagger), \quad (5)$$

in which  $s^\dagger (s)$  and  $d^\dagger (d)$  are the creation (annihilation) operators of  $s$  and  $d$  bosons, respectively. The two pairing operators  $\{\hat{S}_\rho^\pm, \hat{S}_\rho^0\}$  ( $\rho = s, d$ ) satisfy the following commutation relations:

$$[\hat{S}_{\rho'}^0, \hat{S}_\rho^\pm] = \pm \delta_{\rho'\rho} \hat{S}_\rho^\pm, \quad [\hat{S}_{\rho'}^+, \hat{S}_\rho^-] = -2\delta_{\rho'\rho} \hat{S}_\rho^0. \quad (6)$$

For a theoretical framework, a simple IBFM Hamiltonian with the two-configuration mixing term is employed that is based on the even-even boson core coupled with a single fermion in the  $j = 7/2$  orbit. The Hamiltonian of the IBFM can be written as

$$\hat{H} = \hat{H}_B + \hat{H}_F + \hat{V}_{BF} + \hat{H}_{\text{mix}}, \quad (7)$$

where  $\hat{H}_B$ ,  $\hat{H}_F$ , and  $\hat{V}_{BF}$  are the operators for boson, fermion, and interaction between them respectively and  $\hat{H}_{\text{mix}}$  is the two-configuration mixing term.

The operators in Eq. (7) can be defined as

$$\hat{H} = c \left( (1-x)\hat{n}_d + \frac{x}{N}\hat{S}^+\hat{S}^- + y\frac{2x}{N}\hat{Q}_B \cdot \hat{q}_F + \hat{H}_{\text{mix}} \right), \quad (8)$$

where  $x$  is the control parameter for the transition of  $U(5) \otimes U(2j+1) - O(6) \otimes U(2j+1)$ . We must mention that  $x = 0$  and 1 denote the  $U(5) \otimes U(2j+1)$  and  $O(6) \otimes U(2j+1)$  limits, respectively. The generators of the Lie algebra for the quasispin group with  $\hat{S}^+$  and  $\hat{S}^-$  and quadrupole and fermion operators with  $\hat{Q}_B$ ,  $\hat{q}_F$ , and  $\hat{H}_{\text{mix}}$  can be defined as

$$\hat{S}^+ = \hat{S}_d^+ - \hat{S}_s^+, \quad \hat{S}^- = \hat{S}_d^- - \hat{S}_s^-,$$

$$\hat{Q}_B = (s^\dagger \times \tilde{d} + d^\dagger \times \tilde{s})^{(2)},$$

$$\hat{q}_F = (a_j^\dagger \times \tilde{a}_j)^{(2)},$$

$$\hat{H}_{\text{mix}} = g_s \hat{S}_s^+ + g_d \hat{S}_d^+ + g_s \hat{S}_s^- + g_d \hat{S}_d^-. \quad (9)$$

In a normal basis, any quantum state can be represented as a linear combination of  $U(5) \supset O(5) \supset O(3)$ , with a certain angular momentum for the IBFM framework,

$$|J_\xi\rangle = \sum_{n_d \nu \alpha L} C_{n_d, \nu}^{L, \xi} |N n_d \nu \alpha L; n l j; JM\rangle, \quad (10)$$

where  $N n_d \nu \alpha L; n l j; J$ , and  $M$  are the total boson number,  $d$  boson number, seniority number, an additional quantum number to distinguish different states with the same  $L$ , angular momentum, fermion number, orbital quantum number, fermion angular momentum, the total angular momentum quantum number, and third components of the total angular momentum, respectively. Also, the coefficient  $C_{n_d, \nu}^{L, \xi}$  is the corresponding amplitude of the eigenvector obtained by diagonalizing the Hamiltonian. The configuration mixing  $\hat{H}$  under projection operator ( $\hat{P}$ ) in the  $U(5)$  limit of the IBM is then written as  $\hat{H} = \hat{P}(\hat{H}_B + \hat{H}_F + \hat{V}_{BF} + \hat{H}_{\text{mix}})\hat{P}$ . In addition to the mixing parameters  $g_s$  and  $g_d$ , the mixing calculation requires another parameter, which we call the offset parameter ( $\Delta$ ), to excite two more particles from the closed shell. In our previous configuration mixing paper,  $\Delta$  is taken according to the energy of the lowest intruder state to reduce the number of parameters. Here we have the same procedure, and the  $\Delta$  term is fixed at  $\Delta = 0.8$  MeV to promote a proton boson into the next major shell. It should be noted that the Casimir operator of  $O(5)$  and the  $O(3)$  invariant  $L \cdot L$  in the  $U(5)$  Hamiltonian are commutative with  $S_s^\pm$  and  $S_d^\pm$ .  $\hat{P}$ , satisfying  $\hat{P}^2 = \hat{P}$  and  $\hat{P}^\dagger = \hat{P}$ , is the projection operator defined by

$$\begin{aligned} \hat{P} &= |N' n_d \nu \alpha L; n l j; JM\rangle \\ &= \begin{cases} |N' n_d \nu \alpha L; n l j; JM\rangle & \text{if } N' \geq N, \\ 0 & \text{otherwise,} \end{cases} \end{aligned} \quad (11)$$

which keeps the Hamiltonian (7) effective only within the subspace spanned by  $[N] \oplus [N+2] \oplus [N+4] \oplus \dots$  mixed configurations, where  $N$  is the total boson number of the system without configuration mixing, and  $|N' n_d \nu \alpha L; n l j; JM\rangle$  is a basis vector with the total number of bosons  $N' = N + 2n$  with  $n = 0, 1, 2, \dots$

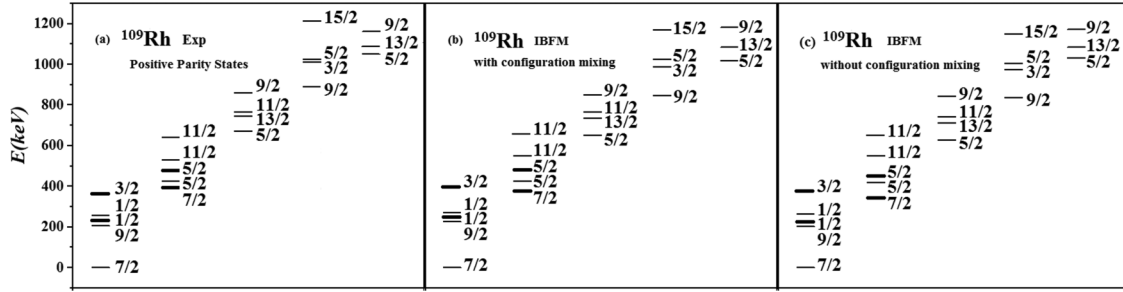


FIG. 3. Partial energy spectra of  $^{109}\text{Rh}$  for positive parity. Experimental data (a) are taken from [22] and references therein. Calculations (b) and (c) are based on the even-even boson core coupled with a single fermion, where thick lines indicate the intruder states. Parameters are taken as  $x = 0.8$ ,  $g_s = -287.16$ ,  $g_d = 88.19$ ,  $z = -108.47$ ,  $c = -0.506$  in keV.

In the IBFM configuration mixing calculation, one needs to consider the basis vector. The lower eigenvalue leads to the following form of the energy matrix:

$$\begin{pmatrix} \langle U(5)_N | U(5)_N \rangle & \langle U(5)_N | H_{\text{mix}} | O(6)_{N+2} \rangle \\ \langle O(6)_{N+2} | H_{\text{mix}} | U(5)_N \rangle & \langle O(6)_{N+2} | O(6)_{N+2} \rangle \end{pmatrix}, \quad (12)$$

where  $U(5)$  symmetry applies on the basis state with  $N$  bosons only, whereas the  $O(6)$  symmetry has to be applied to the states with  $N + 2$  bosons, the total wave function being of the type  $|Nn_d\nu\alpha L; j; J\rangle = |\psi\rangle = J_{\xi_1}|\psi_N\rangle + J_{\xi_2}|\psi_{N+2}\rangle$ . The calculations are performed in two steps. In the first, the Hamiltonian is diagonalized without mixing configuration in the usual basis (right panel of Figs. 3 and 4). In the second,  $\hat{H} + \hat{H}_{\text{mix}}$  is diagonalized with mixing configuration (middle panel of Figs. 3 and 4). In this step an energy  $\Delta$  is also added to the energies of the states of the configuration. Using the commutation relation and diagonalizing  $\hat{H}|\psi\rangle = E_{n_d\nu\alpha L}^\xi|\psi\rangle$ , we can obtain the eigenvalues. Here we employ the same procedure as in [52] to get the energy spectra by diagonalization of the Hamiltonian.

### B. E2 transitions

One important piece of information for the intruder states in connection with band mixing is the transition probabilities [41,42]. E2 transition rates between different excited states (normal and intruder states) provide detailed information about the nuclear structure. As the E2 transitions are very sensitive to band mixing, the calculated transition probabilities are the best evidence for the mixing, which we will discuss in the next section. We define the electric quadrupole operator

as [5,53]

$$T_{\text{IBFM}}^{E2} = e^B [s^\dagger \times \tilde{d} + d^\dagger \times \tilde{s}]_\mu^{(2)} + e^F [a_j^\dagger \times \tilde{a}_j]^{(2)}, \quad (13)$$

where  $e^B$  and  $e^F$  are the effective charges. The E2 transition strength is defined as

$$B(E2; J_i \rightarrow J_f) = \frac{|\langle J_f | \hat{T}_{\text{IBFM}}^{(E2)} | J_i \rangle|^2}{2J_i + 1}, \quad (14)$$

for which we have used the selection rules to obtain the E2 transition rates.

### C. Band mixing

Some prominent phenomena are observed for the neutron-rich nuclei around mass  $A = 100$ – $110$ . These are the band mixing [44–46], shape coexistence [54,55], and existence of the intruder states [15,22,56]. There is a correlation between these phenomena. Venkova *et al.* [17] stated that strong band mixing was expected in  $^{109}\text{Rh}$ , but was not observed. This weak mixing is consistent with the simple analysis in Sec. II above.

To further understand the structural properties of  $^{109}\text{Rh}$ , we have compared experimental results and IBFM calculations.

## IV. NUMERICAL RESULTS

The diagonalization of the Hamiltonian can easily determine eigenenergies. Since the IBM works best for low-lying states, high-lying states are not considered in our IBFM calculation. The model is restricted with even numbers of protons and neutrons. In order to fix the number of bosons one takes

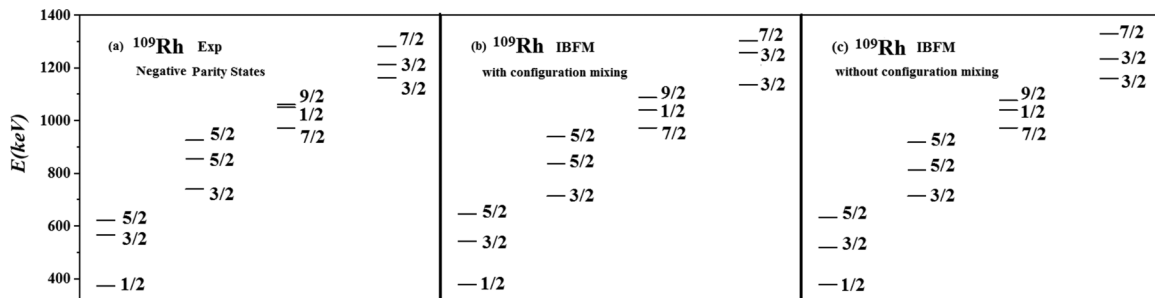


FIG. 4. As in Fig. 3, but for negative parity. Parameters are taken as  $x = 0.8$ ,  $g_s = -250.38$ ,  $g_d = 59.51$ ,  $z = -74.17$ ,  $c = -0.45$  in keV.

into account the nearest closed shell with magic numbers. Here,  $_{40}\text{Zr}_{50}$  is preferred as a closed shell nucleus. In the present IBM calculation, the number of neutron and proton pairs would be  $N_\nu = 7$  and  $N_\pi = 2$ . In the proposed structure, the  $Z = 40$  subshell and  $N = 50$  major shell closures are taken as the inert core, and the intruder configuration represents the proton 2p-2h excitation from the  $g_{9/2}$  orbital. The model is based on the even-even boson core with a quasispin type IBM Hamiltonian coupled with a single fermion. The coupling parameters of the boson-fermion interaction term are extracted separately for positive and negative parity states. The fixed values  $x = 0.8$  and  $y = 1$  for positive and negative parity states are adopted. Figure 1 compares experimental and calculated results. The coupling parameters  $g_s$  and  $g_d$  for  $s$  and  $d$  bosons were all taken to be real with  $g_s > 0$  and  $g_d > 0$ , for example, shown in [57,58], while the configuration mixing Hamiltonian adopted in (7) is equivalent to (8) with  $g_s = -g_d$  in our calculations. In the diagonalization, the mixing Hamiltonian is applied to obtain a low-lying spectrum, and the term  $\hat{H}_L = zJ(J+1)$  is added to (7) to lift the degeneracy of the levels with the same seniority to form the angular momentum sequences with different angular momentum quantum numbers. It is known that in the Hamiltonian, if  $g_s = g_d = 0$ , the system is for the normal IBFM without configuration mixing. With nonzero  $g_s$  and  $g_d$  values, the mixing occurs. We can see that the band structure is basically well reproduced.

Considering the normal and different members of the lowest  $K = 1/2^+$  band, it becomes interesting to search for possible vibrational and rotational bands, respectively, and to compare with theoretical IBFM predictions. Energy spectra for the IBFM calculations are shown in Figs. 3 and 4 for states that are candidates for members of the normal and intruder bands. We can see that  $^{109}\text{Rh}$  is an excellent candidate for triaxiality and shape coexistence because we have  $x = 0.8$ , close to the  $\gamma$ -soft limit. In the last section, we have found that, in  $^{109}\text{Rh}$ , the mixing between the two configurations with  $K = 1/2$  and  $3/2$  is weak for the low-spin  $3/2$  states, resulting in small discrepancies with the experimental data. To shed some light into the origin of the mixing, the sensitivity of the energy spectra to the values of these mixing strength ( $g_s$  and  $g_d$ ), can be noted in Figs. 3 and 4.

We find there are not significant differences between the results in the presence and absence of configuration mixing terms. This implies that the effect of configuration mixing is negligible in  $^{109}\text{Rh}$ . We believe that the configuration mixing scheme is important to find new insights into triaxiality and shape coexistence phenomena. In the present case, configuration mixing has a prominent role in clarifying the rotational contribution in odd mass nuclei. It should be noted that with this approach it is important to get the intruder states. The configuration mixing scheme is applied to describe both normal and intruder states and keeps the lower part of the  $\gamma$ -unstable spectrum unchanged.

It is clear that multiple orbitals are important for the low-lying states. The predicted energies for the  $3/2^+$ ,  $1/2^+$ ,  $7/2^+$ , and  $5/2^+$  intruder levels are 220.28, 232.71, 402.6, and 393.7 keV, to be compared with experimental values of 225.9, 257.7, 409.7, and 478.3 keV, respectively.

TABLE III. IBFM calculations and experimental values of E2 transition rates (W.u) in  $^{109}\text{Rh}$ . The model effective charge parameters are  $e^B = 8.85$  and  $e^F = 29.80$ . Experimental data are taken from [60].

$i$	$f$	E2 (calc)	E2 (exp)
$(3/2)_1$	$(7/2)_1$	0.45	0.0174(5)
$(1/2)_1$	$(3/2)_1$	169.67	170(50)
$(3/2)_2$	$(7/2)_1$	16.59	26.2(5)
$(7/2)_2$	$(3/2)_1$	65.64	136(5)
$(5/2)_1$	$(9/2)_1$	65.57	>23
$(5/2)_2$	$(1/2)_1$	74.07	113(8)
$(5/2)_1$	$(9/2)_1$	23.6	26(3)
$5/2(672)$	$(5/2)_1$	66.17	>150
$5/2(672)$	$(9/2)_1$	23.6	>5.9

The positive-parity states calculated based on the configuration mixing scheme in this work extend above 1 MeV and are consistent with those already noted from previous work [59]. The experimental level scheme of  $^{109}\text{Rh}$  has been deduced from [22] and references therein. For both the normal and  $K = 1/2^+$  [431] bands, experiment and IBFM calculations are in reasonable agreement.

Results of the calculations for E2 transition are listed in Table III and compared with experimental values.

Based on the signatures for shape coexistence reported in [22,51], the intruder states must form a rotational-like band. Comparing the  $K = 1/2$  bands to the calculated level shows an agreement of the IBFM calculations with experimental values. Under the expectation for intruder states, strong E2 intraband transitions should be seen. These transitions are verified by IBFM calculations, connecting the  $K = 1/2^+$  band members in  $^{109}\text{Rh}$ . The agreement is quite reasonable for both the normal and intruder states. The calculations with the present model give a reasonable fit to both excitation energies and E2 transition rates.

In addition to energy spectra and E2 transition strengths, M1 rates are also important observables to compare with results of model calculations. To obtain B(M1) values, the standard operators have been used:

$$T_\mu^{(M1)} = T_{B,\mu}^{(M1)} + T_{F,\mu}^{(M1)}, \quad (15)$$

$$T_{B,\mu}^{(M1)} = \alpha[d^\dagger \times \tilde{d}]_\mu^{(1)}, \quad (16)$$

$$T_{F,\mu}^{(M1)} = \beta[a_j^\dagger \times \tilde{a}_j]_\mu^{(1)}. \quad (17)$$

Based on the Wigner-Ekart theorem, one can calculate the B(M1) values by (15). We have taken  $\alpha = 0.52$  and  $\beta = 0.63$ . A comparison is presented in Table IV. Experimental values are from [22,58]. Overall agreement is reasonable, although many M1 strengths remain to be measured.

## V. CONCLUSION

The triaxiality of the  $^{109}\text{Rh}$  nucleus was studied through IBFM calculations. The experimental energy spectra and

TABLE IV. Calculated and experimental  $B(M1)$  values in  $^{109}\text{Rh}$ . Experimental data are taken from [60].

$E_i$ (keV)	$J_i^\pi$	$E_f$ (keV)	$J_f^\pi$	$B(M1)_{\text{calc}}$ (W.u.)	$B(M1)_{\text{exp}}$ (W.u.)
206.250 (20)	9/2 <sup>+</sup>	0.0	7/2 <sup>+</sup>	0.0102	0.20(3)
358.584 (16)	3/2 <sup>+</sup>	257.66 (3)	3/2 <sup>+</sup>	0.00013	0.00032 (10)
358.584 (16)	3/2 <sup>+</sup>	225.873 (19)	3/2 <sup>+</sup>	0.00110	0.00118 (11)
409.74 (3)	7/2 <sup>+</sup>	206.250 (20)	9/2 <sup>+</sup>	$4.8 \times 10^{-6}$	0.00025 (6)
409.74 (3)	7/2 <sup>+</sup>	0.0	7/2 <sup>+</sup>	$2.6 \times 10^{-5}$	$6.6 \times 10^{-5}$ (8)
426.759 (19)	5/2 <sup>+</sup>	358.584 (16)	3/2 <sup>+</sup>	0.007	0.26(2)
426.759 (19)	5/2 <sup>+</sup>	225.873 (19)	3/2 <sup>+</sup>	0.0008	>0.00040
426.759 (19)	5/2 <sup>+</sup>	0.0	7/2 <sup>+</sup>	0.0007	>0.0032
478.28 (3)	5/2 <sup>+</sup>	358.584 (16)	3/2 <sup>+</sup>	0.0017	0.0025 (4)
478.28 (3)	5/2 <sup>+</sup>	225.873 (19)	3/2 <sup>+</sup>	0.0002	0.0024 (3)
478.28 (3)	5/2 <sup>+</sup>	0.0	7/2 <sup>+</sup>	$1.3 \times 10^{-5}$	$4.1 \times 10^{-5}$ (6)
568.10 (4)	3/2 <sup>-</sup>	373.99 (3)	1/2 <sup>-</sup>	0.0005	
623.12 (4)	5/2 <sup>-</sup>	568.10 (4)	3/2 <sup>-</sup>	0.0050	0.054 (8)
671.876 (22)	5/2 <sup>+</sup>	0.0	7/2 <sup>+</sup>	0.0079	>0.00019
740.80 (4)	3/2 <sup>-</sup>	623.12 (4)	5/2 <sup>-</sup>	0.0039	>0.0065
740.80 (4)	3/2 <sup>-</sup>	568.10 (4)	3/2 <sup>-</sup>	0.0069	>0.015
740.80 (4)	3/2 <sup>-</sup>	373.99 (3)	1/2 <sup>-</sup>	0.060	>0.0058
855.99 (4)	5/2 <sup>-</sup>	740.80 (4)	3/2 <sup>-</sup>	0.0093	>0.017
855.99 (4)	5/2 <sup>-</sup>	623.12 (4)	5/2 <sup>-</sup>	0.0090	>0.017
855.99 (4)	5/2 <sup>-</sup>	568.10 (4)	3/2 <sup>-</sup>	0.0005	>0.0053
861.00 (8)	9/2 <sup>+</sup>	409.74 (3)	7/2 <sup>+</sup>	0.00071	
861.00 (8)	9/2 <sup>+</sup>	0.0	7/2 <sup>+</sup>	0.00001	
926.76 (4)	5/2 <sup>-</sup>	740.80 (4)	3/2 <sup>-</sup>	0.0060	0.0053 (16)
926.76 (4)	5/2 <sup>-</sup>	623.12 (4)	5/2 <sup>-</sup>	0.0073	0.0034 (11)
926.76 (4)	5/2 <sup>-</sup>	568.10 (4)	3/2 <sup>-</sup>	0.0036	0.0016 (6)
1011.60 (4)	3/2 <sup>+</sup>	426.759 (19)	5/2 <sup>+</sup>	$6.3 \times 10^{-8}$	
1026.46 (3)	(5/2, 7/2) <sup>+</sup>	671.876 (22)	5/2 <sup>+</sup>	0.00011	>0.00022
1026.46 (3)	(5/2, 7/2) <sup>+</sup>	426.759 (19)	5/2 <sup>+</sup>	0.00008	>0.00013
1026.46 (3)	(5/2, 7/2) <sup>+</sup>	409.74 (3)	7/2 <sup>+</sup>	$2.4 \times 10^{-5}$	> $6.9 \times 10^{-5}$
1026.46 (3)	(5/2, 7/2) <sup>+</sup>	0.0	7/2 <sup>+</sup>	0.00044	>0.00011
1096.25 (4)	(9/2) <sup>+</sup>	0.0	7/2 <sup>+</sup>	0.00090	
1096.25 (4)	(9/2) <sup>+</sup>	409.74 (3)	7/2 <sup>+</sup>	0.0013	

the two-mixing configuration model calculations are consistent for the low-lying states. In conclusion, the mixing amplitudes confirm the weak nature of the mixing, in particular, the purity of the  $K = 1/2$  intruder band. This work is part of a more systematic study of the  $A \approx 100$  region for which high-lying states should provide more information. We hope that, combined with solvable models, these systematic investigations will allow an understanding of structure of rotational bands in these nuclei. Investigations of high-lying states in neutron-rich isotopes using the same approach are in progress.

#### ACKNOWLEDGMENTS

Support from the National Natural Science Foundation of China (Grants No. 11875171, No. 11675071, and No. 11747318), the U.S. National Science Foundation (Grants No. OIA-1738287 and No. ACI -1713690), U.S. Department of Energy (Grant No. DE-SC0005248), the Southeastern Universities Research Association, the China-U.S. Theory Institute for Physics with Exotic Nuclei (CUSTIPEN) (Grant No. DE-SC0009971), and the LSU-LNNU joint research program (9961) is acknowledged.

[1] A. Arima and F. Iachello, *Ann. Phys.* **99**, 253 (1976).  
[2] A. Arima and F. Iachello, *Phys. Rev. C* **14**, 761 (1976).  
[3] A. Arima and F. Iachello, *Ann. Phys.* **111**, 201 (1978).  
[4] A. Arima and F. Iachello, *Ann. Phys.* **123**, 468 (1979).  
[5] F. Iachello and P. Van Isacker, *The Interacting Boson-fermion Model* (Cambridge University Press, Cambridge, UK, 1991).  
[6] M. Caprio and F. Iachello, *Nucl. Phys. A* **781**, 26 (2007).

[7] C. E. Alonso, J. M. Arias, and A. Vitturi, *Phys. Rev. C* **75**, 064316 (2007).  
[8] F. Iachello, A. Leviatan, and D. Petrellis, *Phys. Lett. B* **705**, 379 (2011).  
[9] K. Nomura, T. Nikšić, and D. Vretenar, *Phys. Rev. C* **93**, 054305 (2016).  
[10] K. Nomura, R. Rodríguez-Guzmán, and L. M. Robledo, *Phys. Rev. C* **96**, 064316 (2017).

- [11] D. Bucurescu and N. V. Zamfir, *Phys. Rev. C* **98**, 024301 (2018).
- [12] E. W. Otten, in *Treatise on Heavy-Ion Science*, Nuclei Far From Stability, Vol. 8, edited by D. A. Bromley (Plenum Press, New York, London, 1989), p. 517.
- [13] J. Hamilton, A. Ramayya, S. Zhu, G. Ter-Akopian, Y. T. Oganessian, J. Cole, J. Rasmussen, and M. Stoyer, *Prog. Part. Nucl. Phys.* **35**, 635 (1995).
- [14] H. Hua *et al.*, *Phys. Rev. C* **69**, 014317 (2004).
- [15] G. Lhersonneau *et al.*, *Eur. Phys. J. A* **1**, 285 (1998).
- [16] K. Heyde, P. Van. Isacker, J. L. Wood, and R. A. Mayer, *Phys. Rep.* **102**, 291 (1983).
- [17] T. Venkova *et al.*, *Eur. Phys. J. A* **6**, 405 (1999).
- [18] H. Abusara, S. Ahmad, and S. Othman, *Phys. Rev. C* **95**, 054302 (2017).
- [19] K. Nomura, R. Rodríguez-Guzmán, and L. M. Robledo, *Phys. Rev. C* **94**, 044314 (2016).
- [20] N. Kaffrell *et al.*, *Nucl. Phys. A* **470**, 141 (1987).
- [21] J. Skalski, S. Mizutori, and W. Nazarewicz, *Nucl. Phys. A* **617**, 282 (1997).
- [22] B. Bucher *et al.*, *Phys. Rev. C* **98**, 064320 (2018).
- [23] W. Dietrich, A. Bäcklin, C. Lannergård, and I. Ragnarsson, *Nucl. Phys. A* **253**, 429 (1975).
- [24] K. Heyde, M. Waroquier, and R. A. Meyer, *Phys. Rev. C* **17**, 1219 (1978).
- [25] Y. X. Luo *et al.*, *Phys. Rev. C* **70**, 044310 (2004).
- [26] Y. Luo *et al.*, *Phys. Rev. C* **69**, 024315 (2004).
- [27] T. Venkova *et al.*, *Eur. Phys. J. A* **15**, 429 (2002).
- [28] K. Nomura, R. Rodríguez-Guzmán, and L. M. Robledo, *Phys. Rev. C* **95**, 064310 (2017).
- [29] N. Gavrielov, A. Leviatan, and F. Iachello, *Phys. Rev. C* **99**, 064324 (2019).
- [30] J.-E. García-Ramos and K. Heyde, *Phys. Rev. C* **100**, 044315 (2019).
- [31] M. Sambataro and G. Molnar, *Nucl. Phys. A* **376**, 201 (1982).
- [32] T. Thomas *et al.*, *Phys. Rev. C* **88**, 044305 (2013).
- [33] J. L. Wood and K. Heyde, *Phys. Rep.* **215**, 101 (1992).
- [34] K. Heyde and J. L. Wood, *Rev. Mod. Phys.* **83**, 1467 (2011).
- [35] F. Pan and J. Draayer, *Nucl. Phys. A* **636**, 156 (1998).
- [36] F. Pan, Y. Zhang, and J. Draayer, *J. Phys. G: Nucl. Part. Phys.* **31**, 1039 (2005).
- [37] F. Pan, Y. Zhang, H.-C. Xu, L.-R. Dai, and J. P. Draayer, *Phys. Rev. C* **91**, 034305 (2015).
- [38] A. J. Majarshin, M. Jafarizadeh, and H. Sabri, *Eur. Phys. J. Plus* **132**, 418 (2017).
- [39] A. J. Majarshin, *Eur. Phys. J. A* **54**, 11 (2018).
- [40] A. J. Majarshin, H. Sabri, and M. Rezaei, *Nucl. Phys. A* **971**, 168 (2018).
- [41] F. Pan, S. Yuan, Z. Qiao, J. Bai, Y. Zhang, and J. P. Draayer, *Phys. Rev. C* **97**, 034326 (2018).
- [42] F. Pan, D. Li, G. Cheng, Z. Qiao, J. Bai, and J. P. Draayer, *Phys. Rev. C* **97**, 034316 (2018).
- [43] A. J. Majarshin, Y.-A. Luo, F. Pan, and J. P. Draayer, *Chin. Phys. C* **45**, 024103 (2021).
- [44] H. T. Fortune, *Phys. Rev. C* **95**, 054313 (2017).
- [45] H. T. Fortune, *Phys. Rev. C* **98**, 064303 (2018).
- [46] K. Wimmer *et al.*, *Eur. Phys. J. A* **56**, 159 (2020).
- [47] F. Pan, D. Zhou, Y. He, S. Yang, Y. Zhang, and J. Draayer, *Phys. Lett. B* **795**, 165 (2019).
- [48] A. J. Majarshin, Y.-A. Luo, F. Pan, H. T. Fortune, and J. P. Draayer, *Phys. Rev. C* **103**, 024317 (2021).
- [49] E. R. Flynn, F. Ajzenberg-Selove, R. E. Brown, J. A. Cizewski, and J. W. Sunier, *Phys. Rev. C* **24**, 902 (1981).
- [50] T. Hagen *et al.*, *Eur. Phys. J. A* **54**, 50 (2018).
- [51] H. Lehmann and J. Jolie, *Nucl. Phys. A* **588**, 623 (1995).
- [52] L. Dai, F. Pan, Z. Feng, Y. Zhang, S. Cui, and J. Draayer, *Chin. Phys. C* **44**, 064102 (2020).
- [53] W. Greiner and J. A. Maruhn, *Nuclear Models* (Springer, New York, 1996).
- [54] G. Lhersonneau *et al.*, *Phys. Rev. C* **49**, 1379 (1994).
- [55] J. Äystö *et al.*, *Nucl. Phys. A* **515**, 365 (1990).
- [56] G. Lhersonneau, J. Wang, S. Hankonen, P. Dendooven, P. Jones, R. Julin, and J. Äystö, *Eur. Phys. J. A* **2**, 25 (1998).
- [57] P. D. Duval and B. R. Barrett, *Phys. Lett. B* **100**, 223 (1981).
- [58] P. D. Duval and B. R. Barrett, *Nucl. Phys. A* **376**, 213 (1982).
- [59] J. Jolie, P. Van Isacker, K. Heyde, J. Moreau, G. Van Landeghem, M. Waroquier, and O. Scholten, *Nucl. Phys. A* **438**, 15 (1985).
- [60] National Nuclear Data Center (Brookhaven National Laboratory), <http://www.nndc.bnl.gov/chart/reColor.jsp?newColor=dm>.